Electronic Structure of Ti3+–Ethylene Complexes in Microporous Aluminophosphate Materials. A Combined EPR and DFT Study Elucidating the Role of SOMO Orbitals in Metal–Olefin π Complexes

Morra, Elena; Cuko, Andi; Maurelli, Sara; Berlier, Gloria; Ugliengo, Piero; Chiesa, Mario. Electronic Structure of Ti3+–Ethylene Complexes in Microporous Aluminophosphate Materials. A Combined EPR and DFT Study Elucidating the Role of SOMO Orbitals in Metal–Olefin π Complexes. JOURNAL OF PHYSICAL CHEMISTRY. C, NANOMATERIALS AND INTERFACES. 119 (46) pp: 26046-26055.
DOI: 10.1021/acs.jpcc.5b09266

The Electronic Structure of Ti^{3+}-Ethylene Complexes in Microporous Aluminophosphate Materials. A Combined EPR and DFT Study Elucidating the Role of SOMO Orbitals in Metal-Olefin π Complexes.

Elena Morra,[†,‡] Andi Cuko,[†] Sara Maurelli,[†] Gloria Berlier,[†] Piero Ugliengo,[†] Mario Chiesa[†*]

[†] Dipartimento di Chimica, Università di Torino and NIS Centre, via P. Giuria 7, 10125, Torino, Italy

[‡] Dutch Polymer Institute (DPI) P.O. Box 902, 5600 AX Eindhoven, The Netherlands

[*] Corresponding Author: e-mail: mario.chiesa@unito.it

The interaction of tetrahedrally coordinated Ti^{3+} ions generated in the framework of TiAlPO-5 microporous materials with $^{12,13}C_2H_4$ leads to the formation of side-on η^2 $\{Ti^{3+}–C_2H_4\}$ complexes with a unique 5-fold coordination of titanium, supported by four oxygen donor ligands of the framework. The detailed electronic and magnetic structure of this adduct is obtained by the combination of advanced EPR techniques (HYSCORE and SMART-HYSCORE) in conjunction with periodic and cluster model DFT calculations. The binding of C_2H_4 results from the σ overlap of low lying C_2H_4 filled π orbitals with the $3d_{z^2}$ empty orbital of titanium, enhanced by a small contribution due the π overlap between the semioccupied $3d_{yz}$ orbital of titanium and the empty π^* orbital of ethylene. The spin density repartition over the ethylene molecule, obtained experimentally, allows probing directly the entity of the metal-to-substrate π^*-back donation, highlighting an asymmetry in the spin density delocalization. This interesting feature is supported by parallel theoretical calculations, which cast the role of the oxygen donor ligands in driving this bonding asymmetry. As a consequence, the interesting structural feature of potential and actual inequality in the electronic spin states (α,β) on the two ethylene carbon atoms of the π coordinated ethylene molecule is produced. The underlying electronic effects associated to the π coordination of ethylene to an early transition metal in paramagnetic state are thus revealed with an unprecedented accuracy for the first time.

INTRODUCTION

The coordination of olefins to transition metal ions (TMI) is one of the crucial elementary steps involved in a number of relevant catalytic processes involving the transformation of unsaturated hydrocarbons. As an example, the widely accepted Cossee-Arlman mechanism[1] for the polymerization of α-olefins with Ziegler-Natta catalysts, features π-coordination of the olefin to the active species, followed by insertion into the metal–alkyl bond through a four-center transition state. Although the intermediacy of a π-complex is widely accepted, it should be emphasized that there is no experimental proof of the existence of a discrete π-complex intermediate for early transition metal systems.[2]

The metal-olefin π-bond is in general described by a synergistic bonding model, introduced by Dewar[3] and by Chatt and Duncanson,[4] involving electron donation from the olefin π-molecular orbital to the metal *d* empty orbital and electron back-donation from the metal to the olefin π^* molecular orbital. The extent and relative importance of substrate-to-metal σ-donation and metal-to-substrate π^*-back donation remains a debated issue[5] as well as the formation of π

complexes *versus* metallacycles having two metal-carbon σ bonds and only a single carbon-carbon bond.[6] An abundant experimental and theoretical literature is available, concerning metals-olefins systems in low-temperature matrixes, in which the metals are in zerovalent state,[7-11] while a much lower number of experimental studies concerns the interaction of olefins with charged metal species.[12-14] Even less explored is the role of paramagnetic TMI and to our knowledge, there is no systematic experimental study of olefin coordination to open-shell TMI. These paramagnetic ions are known to promote selective radical-type transformations potentially exerting important effects in the selectivity through the subtle participation of the Singly Occupied Molecular Orbital (SOMO) to the reaction.[15,16] One important example is provided by Ti^{3+} ($3d^1$, S=1/2) ions, which are believed to play a crucial role in Ziegler Natta catalysis[17] and many other important catalytic processes.

Recently we have demonstrated that Ti^{3+} species can be easily generated at well defined single sites of microporous aluminophosphates (AlPOs) materials,[18] providing unique models to probe the reactivity of these chemical species.

AlPOs are zeolite-like materials in which silicon ions are replaced by phosphorus and aluminum in strict alternation, forming a 3-dimensional neutral oxide network that can adopt a range of polymorphic structures.[19] In these materials, Al and P ions can be isomorphically replaced by di-, tri-, and tetra-valent heteroatoms in a relatively easy and controllable manner, giving rise to acid, redox, and even bifunctional properties.[20] When activated via the inclusion of dopant ions in the framework, AlPOs have widespread applications in the field of heterogeneous catalysis,[21-23] combining the reactivity of the redox-active cations with high surface area and the unique spatial constraints imposed by the molecular dimensions of their porous network.[24-26] Divalent heteroatoms in MeAlPOs preferentially substitute trivalent Al framework ions at tetrahedral sites, resulting in a Brönsted functionality (necessary to compensate the negative charge delocalized on the framework) which disappears after a reversible oxidation to the trivalent state.[27-31] More complex is the situation when tetravalent ions are inserted in the AlPOs framework, as in the case of Ti^{4+} or V^{4+} ions. Simple chemical considerations would suggest the idea that both ions are substituting for pentavalent P atoms, generating a negative charge on the framework stabilized by a Al(OH)Me Brönsted site.[32-36] However, recent studies gave clear-cut evidence for isomorphous substitution of tetravalent titanium and vanadium ions at both P and Al sites, with emphasis on the presence of reducible Ti ions at Al sites in TiAlPO-5.[18,37-39]

The AlPO-5 structure (AFI) and the specific site considered in this study are shown in Figure 1.

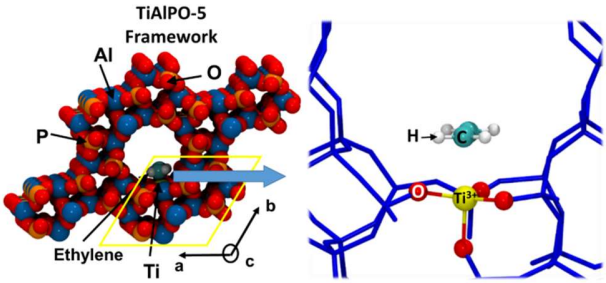

Figure 1. View along the c axis of the Ti-doped AlPO periodic model. Left: 3D space filling model of a framework portion. Right: stick model of framework evidencing the Ti^{3+} tetrahedral site onto which the ethylene molecule is adsorbed. Optimized cell parameters are: a=13.8 Å, b=13.9 Å, c=8.4 Å, α=90.1, β=90.5, γ=120.6. The cell composition is $H_4C_2O_{48}Al_{11}P_{12}Ti_1$.

The presence of easily reducible titanium ions at tetrahedral sites is a unique feature of these materials[40] and is of interest in the context of the study of the chemical reactivity of open shell TMI towards different adsorbates. In particular in this study we are interested at elucidating the electronic and geometric structure of ethylene-Ti^{3+} complexes. To do so, we combine experimental data obtained by CW and pulse EPR techniques with DFT modelling, providing a detailed description of the coordination geometry and the electronic and magnetic structure of mono-ethylene complexes with trivalent titanium, produced by adsorption of C_2H_4 on reduced TiAlPO-5 zeotype materials. The motivation lies in the important role played by open shell Ti^{3+} compounds in catalytic processes such as olefins polymerization in Ziegler Natta catalysis and the small amount of data relative to olefinic C=C double bonds coordinated to Ti^{3+} centres. Emphasis is placed in exploring the underlying electronic effects exerted by singly occupied metal *d*-orbitals in olefin coordination which may serve as a lead for more complex systems.

MATERIALS AND METHODS

Sample preparation

TiAlPO-5 was prepared by hydrothermal synthesis as described elsewhere.[18] Calcined samples were dehydrated under vacuum by gradually raising the temperature to T = 673 K over a period of 2 h and kept at that temperature for 1 h. The dehydrated samples were then reduced under 100 Torr of H_2 at T = 673 K. Gradual pressures of ethylene, from 3 mbar to 10 mbar, were delivered on the reduced sample at T = 77 K. Carbon-13 enriched ethylene (99 atom %^{13}C) gas was purchased from Sigma-Aldrich.

EPR characterization

X-band CW EPR spectra were detected at T = 77 K on a Bruker EMX spectrometer (microwave frequency 9.46 GHz) equipped with a cylindrical cavity. A microwave power of 10 mW, a modulation amplitude of 0.3 mT and a modulation frequency of 100 KHz were used. Pulse EPR experiments at X-band (microwave frequency 9.76 GHz) were performed at T = 10 K on an ELEXYS 580 EPR Bruker spectrometer equipped with a liquid-helium cryostat from Oxford Inc. The magnetic field was measured by means of a Bruker ER035 M NMR gauss meter.

Electron-spin-echo (ESE) detected EPR experiments were carried out with the pulse sequence: $\pi/2 - \tau - \pi - \tau - echo$. Pulse lengths $t_{\pi/2}$ = 16 ns and t_{π} = 32 ns, a τ value of 200 ns and a 1 kHz repetition rate were used.

Hyperfine Sublevel Correlation (HYSCORE) experiments[41] were carried out with the pulse sequence $\pi/2 - \tau - \pi/2 - t_1 - \pi - t_2 - \pi/2 - \tau - echo$. The microwave pulse length $t_{\pi/2}$ = 16 ns and t_{π} = 16 ns were adopted. The time intervals t_1 and t_2 were varied in steps of 8 ns starting from 96 ns to 2496 ns. In order to avoid blind spot effects different τ values were chosen, which are specified in the figure captions. The adopted shot repetition rate was 1 kHz. A four-step phase cycle was used for eliminating unwanted echoes.

The SMART (Single MAtched Resonance Transfer) HYSCORE[42,43] sequence is $p_M - t_1 - \pi - t_2 - p_M - \tau - \pi - \tau - echo$ (p_M = high-turning angle, HTA, matched pulse). The matching-pulse field strength, ν_1, was taken to be 15.0724 MHz. The length of the matching pulse was optimized using a matched three pulse ESEEM experiment.[43] The optimal value was found to be 120 ns (see Figure 1S supporting information). The length of the π pulses was taken to be 16 ns. A four-step phase cycle was used to eliminate unwanted echoes.

The time traces of the HYSCORE spectra were baseline corrected with a third-order polynomial, apodized with a Hamming window and zero filled. After two dimensional Fourier transformation, the absolute value spectra were calculated.

EPR and HYSCORE spectra were simulated using Easyspin.[44]

DFT calculations

We simulated the TiAlPO-5 structure using periodic models that are more suitable than molecular fragments to represent the extended crystalline environment of the TMI ions.[45] The periodic calculations were performed using the CRYSTAL14 software package[46,47] considering a single Ti^{3+} center per unit cell in the AlPO-5 framework at Al^{3+} sites compatible with the experimental findings. The calculations were done within the Density Functional Approximation (DFT) adopting the hybrid Becke, three parameters, Lee-Yang-Parr (B3LYP) functional.[48,49]

The wave function of the systems is described as a linear combination of atomic orbitals expressed as a contraction of Gaussian-type functions. A triple-valence plus polarization basis set for Ti, a double valence plus polarization basis set for P, Al and O, and a single valence plus polarization basis set for H were used during the geometry relaxation of both atomic coordinates and cell vectors. All these basis set are available on the online library of the CRYSTAL14 code. For the electronic and magnetic properties, a single point calculation with the same method was performed using the Ahlrichs triple-ζ plus polarization basis set for all atoms. Furthermore, for Ti and Al atoms, the basis function with exponents lower than 0.06 are removed, to avoid basis set linear dependence (see Table S2 of the supplementary information for details and references).

The Gauss–Legendre quadrature and Lebedev schemes are used to generate angular and radial points of a pruned grid consisting of 75 radial points and 974 angular points over which electron density and its gradient are integrated. Values of the tolerances that control the Coulomb and exchange series in periodical systems [CRYSTAL14 Manual] were set to default values (6 6 6 6 12). The Hamiltonian matrix was diagonalized in 8 k-points (shrink factor = 2) of the first Brillouin zone. The eigenvalue level-shifting technique was used to lock the system in a non-conducting state. The level shifter was set to default value (0.6 Ha) without locking the wavefunction solution up to the end of the self consistent field. To help convergence of the SCF, the Fock/KS matrix at a cycle was mixed with 30% of the one of the previous cycle. The difference between the number of α and β electrons (spin of the systems) for Ti atom is locked to 1 for all the SCF cycles of the calculation. This is strictly necessary in order to obtain the titanium atom under the doublet state in the periodic system.

Harmonic frequencies for ethylene atoms were calculated with CRYSTAL14 at Γ point and the infrared intensity for each normal mode was obtained by computing the dipole moment variation along each normal mode.

The periodic DFT study has been complemented with molecular cluster calculations, performed using the ORCA code,[50] in order to estimate the $\boldsymbol{g}$-tensor of Ti^{3+} that cannot be calculated with CRYSTAL14. A cluster including Ti and its first coordination sphere has been cut out from the optimized periodic structure obtained with CRYSTAL14, as represented in Figure 2.

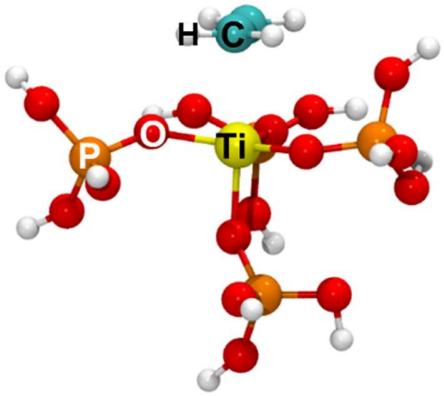

Figure 2**.** View of 3D balls and sticks cluster model of Ti-site in interaction ethylene molecule. Cluster structure is cut from the optimized periodic model. The resulting unsatisfied valences have been saturated with H atoms oriented along the broken bonds. The cluster has net charge=+3 in a doublet spin state.

The resulting unsatisfied valences have been saturated with H atoms oriented along the broken bonds. The net charge on the cluster was set to +3 in a doublet spin state. This charge ensures a good representability of the cluster with respect to the periodic model, as judged by the closeness of the Ti spin density values. The ***g*** tensor has been calculated keeping the atom coordinates fixed, i.e. maintaining Ti and its local environment as in the optimized periodic model.

Since hyperfine interaction (*hfi*) values and a_{iso} in particular are known to be very sensitive to the exchange functional employed, calculations have been repeated with the PBE0 [51] functional, which was found to provide results in better agreement with the experiment. A specifically developed for EPR/NMR magnetic properties Gaussian basis function is utilized for describing the cluster system. The CP(PPP) [52] basis set is adopted for Ti atom, IGLO-II [53] for P atoms and EPR-II [54] for O and H atoms. For the numerical integration of the electron density, 434 points in according with Lebedev scheme are chosen. The SCF convergence criteria are set to 10^{-8} Ha.

RESULTS AND DISCUSSION

EPR Characterization

A typical EPR spectrum of TiAlPO-5 reduced in H_2 atmosphere at 673 K is shown in Figure 3a together with the corresponding computer simulation (dotted line). The spectrum is characterized by two overlapping species (Table 1) with a nearly axial ***g*** tensor typical for Ti^{3+} ions under a distorted tetrahedral symmetry. Clear evidence for isomorphous substitution at Al^{3+} sites is provided by HYSCORE spectroscopy, which allows detecting ^{31}P hyperfine interactions typical for Ti-O-P coordination and only small couplings to remote ^{27}Al nuclei. A typical HYSCORE spectrum recorded at the observer position indicated in Figure 3a is shown in Figure 3c. The spin Hamiltonian parameters relative to the different ^{31}P nuclei were determined and discussed in a previous work.[18]

Adsorption of ethylene (Figure 3b) leads to the modification of the EPR spectrum and a new EPR active species is observed, characterized by the ***g*** tensor reported in Table 1. The spectral change is reversible and pressure dependent (Figure 2S supporting information) and is clearly correlated to the ethylene coordination and subsequent crystal field modification at the Ti^{3+}

metal centre. A more detailed description of ethylene coordination is obtained by means of HYSCORE spectroscopy.

HYSCORE is a two-dimensional experiment where correlation of nuclear frequencies in one electron spin (m_S) manifold to nuclear frequencies in the other manifold is created by means of a mixing π pulse. The HYSCORE spectrum recorded upon ethylene adsorption (Figure 3d) shows ^{31}P and ^{27}Al cross peaks, which are similar to those observed for the reduced sample prior gas adsorption.[18] In addition a ridge in the (+,+) quadrant, centered at about 15 MHz (the ^{1}H Larmor frequency) with a width of about 7 MHz is observed. This signal is not present in the reduced sample (Figure 3c) and can clearly be ascribed to the interaction of the unpaired electron - mainly localized on Ti^{3+}- with the ethylene protons. Double quantum (*DQ*) peaks centered at about twice the ^{1}H Larmor frequency are barely visible in the spectrum (not shown). In order to enhance these features - corresponding to correlations between sum frequencies of the different ethylene protons interacting with the unpaired electron - we recorded SMART HYSCORE spectra at different observer positions (Figure 4). This detection scheme combines the enhanced sensitivity due to the use of matched pulses with the lack of blind spots, allowing the observation of cross peaks at frequencies ($\nu_{1,\alpha}+ \nu_{1,\beta}$, $\nu_{1,\beta} + \nu_{1,\alpha}$) due to correlation of double quantum (*DQ*) coherences. In the spectra of Figure 4, in addition to the strong ridge around ν_H, (evidenced by the dotted red line) corresponding to the correlations between the basic frequencies of the two m_S manifolds, a ridge is also present around $2\nu_H$, which corresponds to correlations between sum frequencies. These sum frequency ridges are particularly informative as they allow determining the relative sign and orientation of the hyperfine tensors. In addition to the ridges correlating proton frequencies, combination peaks involving the sum and difference frequencies of protons with ^{27}Al and ^{31}P are also observed as indicated in Figure 4a (blue dotted lines). The proton hyperfine couplings are particularly informative on the adsorption geometry, however the ridges around ν_H do not allow for the determination of the two tensors and their relative sign and orientations. This information can be obtained by the analysis of the *DQ* ridges. We simulated the shape of the combination-frequency ridges assuming different couplings and orientations of the contributing protons. The simulation analysis indicates that the shape and extension of the *DQ* ridges can be reproduced assuming two interacting protons with slightly different couplings (Table 1). In Figure 4 the correlation ridges of the two protons at ν_H are plotted in red and green and they overlap almost completely. The combination frequencies at $2\nu_H$ are plotted in black.

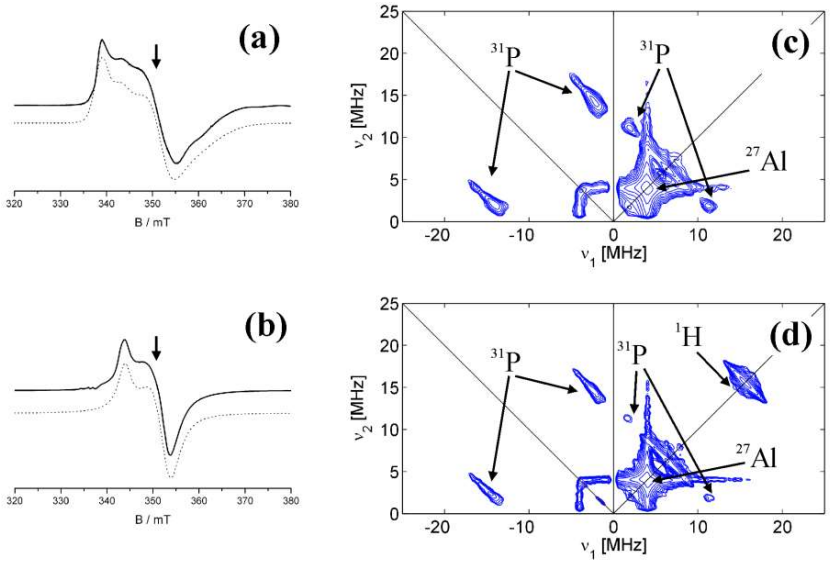

Figure 3. a), b) Experimental (solid line) and simulated (dotted line) CW-EPR spectra of Ti^{3+} species generated in TiAlPO-5 upon (a) reduction in H_2 at 673 K and (b) delivery of 10 mbar of ethylene; c), d) HYSCORE spectra recorded at the magnetic field position corresponding to the arrow in spectra (a) and (b), respectively. The spectra refer to (c) reduced TiAlPO-5 and (d) reduced sample upon delivery of 10 mbar of ethylene. For both the spectra the adopted τ value is 104 ns. The spin Hamiltonian parameters extracted from the computer simulations are reported in Table 1.

Table 1. Spin Hamiltonian parameters derived from computer simulations of Figures 3-5.

		g_x	g_y	g_z		A_x	A_y	A_z	a_{iso}	T_x	T_y	T_z	β	Ref.
Reduced TiAlPO-5	S1	1.898 ±0.005	1.918 ±0.005	1.991 ±0.002										18
	S2	1.969 ±0.002	1.90 ±0.01	1.90 ±0.01										
Reduced TiAlPO-5 + C_2H_4		1.902 ±0.005	1.925 ±0.005	1.964 ±0.002	^{1}H(1)	-3.2 ±0.3	-3.2 ±0.3	6.5 ±0.3	0.0 ±0.3	-3.2 ±0.1	-3.2 ±0.1	+6.4 ±0.1	20±10	This work
					^{1}H(2)	-2.5 ±0.3	-2.5 ±0.3	7.0 ±0.3	+0.7 ±0.3	-3.2 ±0.1	-3.2 ±0.1	+6.4 ±0.1	70±10	
					^{13}C(1)	-1.7 ±0.3	-1.7 ±0.3	1.9 ±0.5	-0.5 ±0.4	-1.2 ±0.1	-1.2 ±0.1	+2.4 ±0.1	-40±20	
					^{13}C(2)	-0.55 ±0.3	-0.55 ±0.3	4.1 ±0.2	+1.0 ±0.3	-1.55 ±0.1	-1.55 ±0.1	+3.1 ±0.1	80±10	

The hyperfine coupling constants are expressed in MHz and the arbitrary convention $g_x<g_y<g_z$ is chosen. The signs of the hyperfine tensor elements were chosen in accordance with the results of the DFT calculations. The Euler angle β, in degrees, relates the orientation of the A_z component with the g_z tensor element.

The best fit was obtained assuming that the two tensors are non-coaxial with respect to the g_z axis, forming angles of approximately 70 and 20 degrees, respectively. The parameters obtained from the simulation of the SMART HYSCORE spectra have been used to simulate the standard ^{1}H HYSCORE spectra (Figure 3S supporting information).

The isotropic and dipolar components of the $A(^1H)$ tensors can be obtained by conventional decomposition ($\boldsymbol{A} = a_{iso}\mathbf{1} + \boldsymbol{T}$), where $\mathbf{1}$ represents the unit matrix. This leads to virtually the same dipolar term for the two protons (T = 3.2 ± 0.6 MHz) and $a_{iso} \approx 0.03$ and 0.7 MHz for $H_{(1)}$ and $H_{(2)}$ respectively, where the sign has been chosen consistently with the positive g_n value of ^{1}H. Considering a purely dipolar interaction the Ti-H distance can be estimated to be 0.29 ± 0.01 nm from the following equation:

$$T = \frac{\mu_0}{4\pi} g_e g_n \beta_e \beta_n \frac{1}{r^3} \qquad (1)$$

with r being the distance between the unpaired electron localized in the Ti d orbitals and the ^{1}H nucleus. This experimentally derived distance is in excellent agreement with the DFT computed one (*vide infra*).

In order to thoroughly characterize the ethylene coordination to Ti^{3+} and the relative spin density transfer, HYSCORE experiments were performed with ^{13}C-enriched ethylene. HYSCORE spectra were recorded at different magnetic fields (Figure 5) and at a τ value that suppresses the contribution of remote ^{27}Al and ^{13}C ions that have similar nuclear Larmor frequencies (ν_{13C} = 3.74796 MHz and ν_{27Al} = 3.88610 MHz at 350 mT).

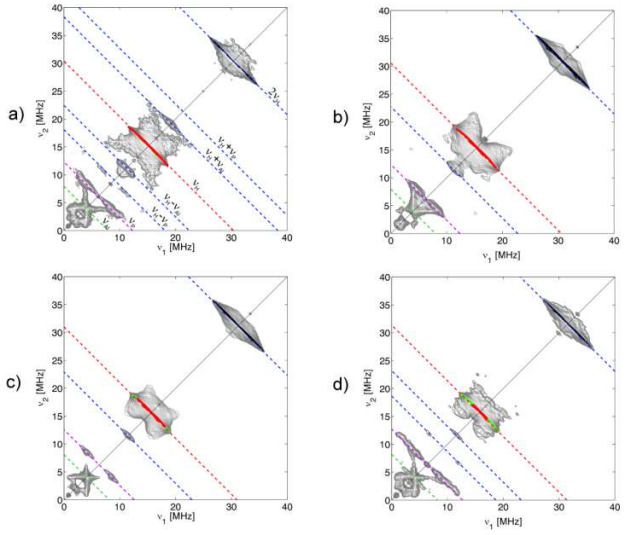

Figure 4. ^{1}H SMART HYSCORE spectra of reduced TiAlPO-5 contacted with 10 mbar of ethylene. The spectra are taken at observer positions corresponding to (a) B_0 = 354.0 mT, (b) B_0 = 359.0 mT, (c) B_0 = 364.0 mT and (d) B_0 = 368.5 mT. The spectra were recorded using τ = 176 ns and symmetrized to obtain a better comparison with the simulations. The simulations of the correlation ridges expected for a three-spin system, S = 1/2, I_1 = 1/2, I_2 = 1/2 assuming the hyperfine couplings reported in Table 1 are superimposed on the experimental spectra. The ^{27}Al, ^{31}P and ^{1}H Larmor frequencies are indicated by the green, magenta and red dotted lines respectively. Combination frequencies are indicated by the dotted blue lines.

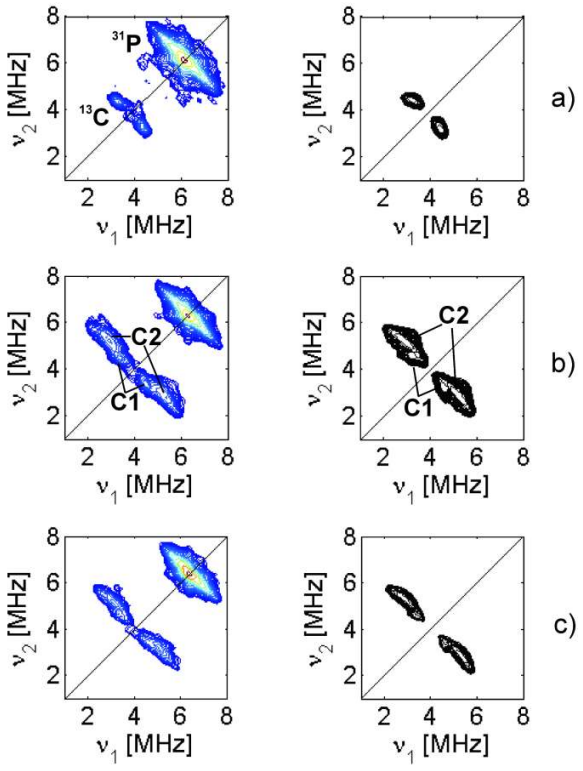

Figure 5. Experimental (color) and computer simulation (black) ^{13}C HYSCORE spectra of TiAlPO-5 upon delivery of 10 mbar of ^{13}C-enriched ethylene. The spectra are recorded at T = 10 K with τ = 250 ns at field positions corresponding to the ESE spectrum turning points, namely (a) B_0 = 355.0 mT, (b) B_0 = 364.7 mT and (c) B_0 = 369.0 mT. The parameters adopted for the simulations are listed in Table 1. Only the ^{13}C signal is simulated.

The spectra are characterized by the presence of cross peaks (C2) centred at the ^{13}C nuclear Larmor frequency, which are absent in the non-enriched system. The maximum coupling (≈ 4 MHz) is observed at magnetic field settings where mainly spectral components associated to g_x and g_y positions of the ESE powder pattern are selected by the HYSCORE experiment. Experiments carried out at the g_z spectral position (Figure 5a) indicate a maximum coupling along this direction of about 1.5 MHz. Careful examination of the spectra reveals that, at field positions corresponding to $g_{x/y}$, a second pair of cross-peaks (C1) is present, located close to the diagonal. These features are no longer observed in the HYSCORE spectrum recorded at the g_z component where they overlap with the C2 signal. The presence of two distinct ^{13}C couplings is confirmed by the simulation analysis, which indicates that no satisfactory fitting of the spectra can be obtained assuming a single ^{13}C coupling. The simulation of the HYSCORE spectrum was thus carried out assuming a three spin system (S=1/2, I(C1)=1/2, I(C2)=1/2). The geometrical constraints derived from DFT modelling (vide infra) were used to estimate the dipolar coupling. A nearly equivalent Ti-C distance of 2.61 Å and 2.65 Å is computed for the two ethylene carbon atoms, which translates into an anisotropic hyperfine component T=1.1 MHz (eq.1). These values were used as starting parameters and changed together with the β Euler angles for the two ^{13}C nuclei until a satisfactory fit was obtained for all observer positions. The result is reported in Figure 5 and the corresponding spin Hamiltonian parameters are listed in Table 1.

Decomposition of the $A(^{13}C)$ tensors leads to $T(C1)$ = 1.2±0.1 MHz and $T(C2)$ = 1.5±0.1 MHz in good agreement with the initial guess. The derived isotropic hyperfine components are found to be $a_{iso}(C1)$= -0.5±0.3 MHz and $a_{iso}(C2)$= 1.0±0.1 MHz where the sign has been chosen in accordance with the positive principal value of the dipolar coupling for 2*p* orbitals and positive g_n value for the ^{13}C nucleus [55] and in agreement with the DFT results. The large dipolar character of the ^{13}C ***A*** tensor is in agreement with the shift of the ridges from the ν_1=-ν_2 axes [56] and its analysis indicates a minute spin delocalization on the ethylene molecule. Moreover the different sign of the isotropic contact term for the two carbon nuclei suggests an asymmetry in the spin delocalization pathway over the adsorbed molecule.

In order to clarify the nature of the $\{Ti^{3+}–C_2H_4\}$ adduct and to develop a detailed self-consistent description of the electronic and molecular structure of the monoethylene complex, corroborative DFT calculations were carried out.

DFT Calculations. Electronic structure and binding mechanism of $\{Ti^{3+}–C_2H_4\}$

The considered model has been based on the experimental findings discussed above, (Figure 3) and consists of a single Ti^{3+} ion per unit cell replacing for an Al^{3+} framework ion. Consistently with the reversibility of the interaction, DFT calculations at B3LYP level (no dispersion included) reveal that the $\{Ti^{3+}–C_2H_4\}$ adduct results unbound with ΔE^C = 3.6 kcal·mol^{-1} (see Table S1). Decomposition of ΔE^C in different energy contributions reveals a large energetic cost associated to the geometrical deformation of the Ti^{3+} centre (δE_S = 9.0 kcal·mol^{-1}) (see Figure 6 for geometrical details) upon ethylene binding, together with a negligible deformation cost of the ethylene (δE_M = 0.4 kcal·mol^{-1}) molecule. However, the interaction energy between the already deformed system gives ΔE^{*C}= -5.8 kcal·mol^{-1} (spontaneous process), showing a weak chemical interaction. When the calculations are repeated by including the dispersive contribution with B3LYP-D*, the system becomes bound with a final interaction energy of ΔE^{CD} = -7.6 kcal·mol^{-1}. In conclusion, while the role of dispersion interactions is essential to keep the system in place at low temperature, it is the chemical interaction which is responsible of the large geometrical restructuring of the Ti^{3+} site and of the spin density transfer towards the ethylene molecule.

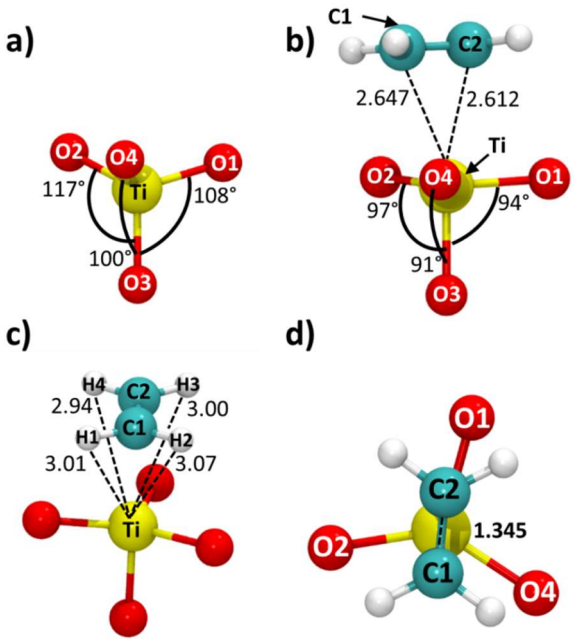

Figure 6. B3LYP optimized a) and b) Ti-site of the periodic model before and after the ethylene adsorption respectively. Ox-Ti-O3 angles are reported in order to emphasize the deformation of Ti-site. c) and d) different views of the periodic Ti-site in which the distances Ti-H and C=C are reported, respectively. All distances are reported in Angstrom.

Upon ethylene ligation the titanium ions attain a five-fold coordination, featuring the side-on ligated C_2H_4 moiety with the distance of the two C atoms to the metal center of 2.647 Å and 2.612 Å. The C–C bond length of the adsorbed C_2H_2 moiety is elongated to 1.345 Å with respect to the free molecule (1.336 Å) suggesting a small weakening of the C-C bond upon binding. This is in agreement with the computed red shift of the C-C bond, which becomes slightly activated upon binding with a bathochromic shift of 25 cm^{-1}. As no experimental spectrum has yet been recorded despite our attempts we deposit the B3LYP computed IR spectrum as supporting information (Figure 4S) for future reference and elaborations. The computed Ti-H distances (Figure 6c) range between 2.94 Å and 3.07 Å, in excellent agreement with those derived from the analysis of the ^{1}H SMART HYSCORE spectra.

We find an interesting result through the topological analysis of the electron density distribution and the evaluation of the critical points.[57] The critical points are locations where the gradient of the electron density is zero and allow the identification of bond paths. In our case we find a single critical point between the Ti^{3+} cation and the midpoint of the C-C bond (Figure 7d), implying a T-shaped electronic structure of the {Ti^{3+}–C_2H_4} adduct. A similar result was found in the theoretical analysis of the $Cu(C_2H_4)^+$ complex.[10]

Table 2. Cluster PBE0 computed *g* and periodic B3LYP ^{1}H and ^{13}C *hfi* tensor elements relative to the model structures illustrated in Figures 1 (*A* tensor) and 4 (*g* tensor).

g_x	g_y	g_z		a_{iso}	T_x	T_y	T_z
1.9443	1.9609	1.9770	$^{1}H1$	+3.1	-2.5	-3.1	+5.6
			$^{1}H2$	+1.5	-2.4	-3.0	+5.4
			$^{1}H3$	-1.4	-2.3	-3.8	+6.1
			$^{1}H4$	-0.6	-2.1	-4.0	+6.1
			$^{13}C1$	-1.3	-1.1	-1.2	+2.3
			$^{13}C2$	+1.5	-3.0	-3.2	+6.2

All the values are given in MHz. The numbering of the atoms is given in Figure 6.

The computed ***g*** and *hfi* tensors for the {Ti^{3+}–C_2H_4} adduct are listed in Table 2. The calculated ***g*** factors, obtained with cluster calculations, qualitatively reproduce the experimental values as well as the *g* shift experimentally observed upon adsorption of ethylene to the naked Ti^{3+} ions (Figure 5S of supporting information).

Comparison of the experimental and DFT calculated ^{1}H hyperfine constants indicates a good agreement in particular between the dipolar tensor components, which are much more sensitive to the structural rather than computational details and much more faithful reporters of the equilibrium structure of the paramagnetic complex. The four protons are found to have very similar dipolar components and different orientations with respect to the ***g*** frame. The full set of Euler angles obtained with the cluster approach is reported as supporting information (Table 1S) together with a simulation of the experimental ^{1}H HYSCORE spectra obtained using the computed values (Figure 6S). The good agreement with the experimental data strongly validates the computational model. In the case of the ^{13}C hyperfine couplings the two carbon nuclei are found to be inequivalent, with C2 displaying a larger coupling in agreement with the larger fraction of (positive) spin delocalization and with the experimental findings. The *hfi* is very sensitive to both computational parameters (method, basis set quality, numerical accuracy, etc) and geometry. This is particularly true in the present case in which the absolute *hfi* values are rather small. The computed *hfi* are slightly overestimated with respect to the experiment and are found to depend critically on the ethylene adsorption geometry as demonstrated by rigid rotations and translations of ethylene with respect to the position assumed in the optimized structure (Figure 7S supporting information). Energetic data of Figure 7S reveal that only small translations of ethylene with respect to the adsorption site are compatible with the low temperature of the experiment, the rotation implying a higher energetic cost. Detailed computed data (not shown) reveal, however, that the anisotropic component of the *hfi* are far less sensitive to the change in the conformation of the adduct. The principal axes of the ^{13}C hyperfine tensor are non-collinear with the ***g*** tensor axes, with the A_z direction of C2 being rotated nearly about $\beta = 90^{\circ}$ along the g_x direction. For the C1 carbon the A_z component is computed to be tilted of $\beta = -45^{\circ}$ with respect to g_z (Figure 8S supplementary information). These computed orientations were used as starting values to simulate the experimental HYSCORE spectra reported in Figure 3.

The origin of the magnetic inequivalence of the two C ethylene atoms can be understood considering the spin density and the HOMO-SOMO plots shown in Figure 7. Visual examination of the HOMO shows that the doubly occupied π bonding orbital of ethylene is engaged with a $3dz^2$ Ti empty orbital in a typical σ donating bond interaction. On the other hand the SOMO is characterized by a dominant $3d_{yz}$ Ti character with a partial overlap to the antibonding π^* orbital of ethylene. However, as a result of the asymmetry introduced by the in plane oxygen (O1), we find an increased orbital population for C2. This translates in a decrease of the Ti-C2 bond length and into a larger amount of α spin transferred in C2 with respect to C1. In turn, β spin is induced in C1 via spin polarization of the σ C-C bond as shown in the spin density plot of Figure 7c, consistently with the experimental observation of two inequivalent C atoms. As an overall the experimental spin Hamiltonian parameters are well reproduced indicating that the calculated SOMO and associate spin density distribution accurately describe the delocalization of the unpaired electron.

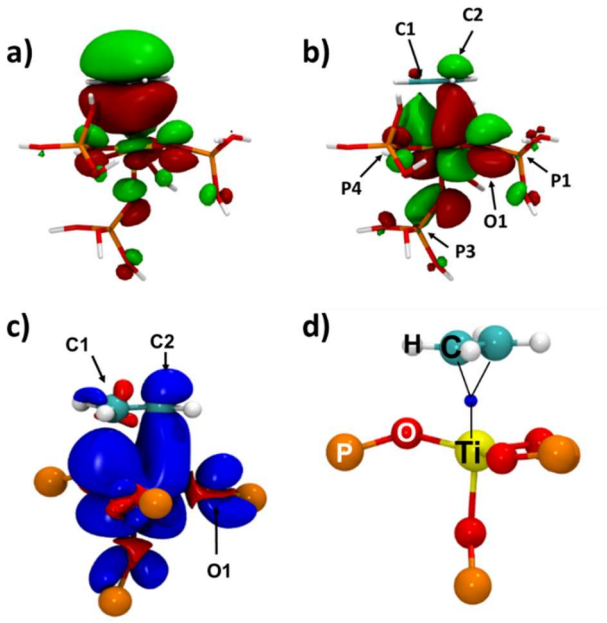

Figure 7. PBE0 a) HOMO and b) SOMO respectively plotted on the cluster structure (contour level 0.02). c) spin density plotted on the periodic structure (blue: α spin, red: β spin, isovalue: 0.0004). d) critical point (blue) of the Bader topological analysis of electron density in the periodic system.

CONCLUSIONS

The olefinic complex between ethylene and Ti^{3+} was experimentally isolated reacting Ti^{3+} ions generated in the AlPO-5 structure with ethylene. From the combination of advanced EPR techniques and DFT periodic calculations a detailed description of the coordination of ethylene to tetrahedrally coordinated Ti^{3+} ions was achieved. Ethylene coordinates to Ti^{3+} ions via a classical donor-acceptor scheme typical for π coordination of olefins. The complex has a T shaped structure and a modest binding energy compatible with the experimentally observed reversibility of the adsorption phenomenon. Although the interaction can be classified as a simple physisorption from the overall energetical point of view, electron transfer channels are clearly evidenced, which result in a small elongation of the C-C bond. The small activation of the C-C bond with respect to other transition metal

ions[5] can be explained considering the small role of π^* back-donation from the metal to the ethylene molecule. This is directly monitored by the spin density transfer and relative ^{13}C hyperfine interactions measured by means of HYSCORE spectroscopy. Interestingly an asymmetry in the spin density transfer towards the two ethylene carbon atoms is observed, which can be traced back to the local structure of the complex featuring the non-innocent role of the solid framework into which the TMI is embedded. This asymmetry in the π^* back-donation produces the interesting consequences of the inequality in the metal-olefinic carbon bond lengths and opposite spin states on the two ethylene carbon atoms. The effect is small but sizable and is related to the geometrical structure of the site. Although at the moment it may appear a chemical oddity associated to this specific system, this spin asymmetry, may have interesting consequences on the chemical reactivity of the ethylene molecule and the steroselectivity of polymerization catalysts. The impact of electronic effects associated to the presence of singly occupied molecular orbital has been so far disregarded in the field of olefin polymerization, however TMI in paramagnetic states feature large in both heterogeneous and homogeneous polymerization catalysis. In these reactions intermediate bond breaking, and further bond making is involved and the spin state of the reactant may have an impact in directing the stereoselectivity of the catalyst. Moving from the evidence provided from the present study, it will be interesting to explore the effect of the chemical nature and the geometrical arrangement of coordinating ligands in modulating the spin repartition on paramagnetic metal-olefin complexes and its potential impact on olefin reactivity.

ASSOCIATED CONTENT

Supporting Information. 3P-ESEEM experiments, pressure dependence of EPR spectra, ^1H HYSCORE simulations, cluster model computed *hfi* tensors and g tensor orientations, computed *hfi* dependence on ethylene geometry, calculated interaction energy of the $\{Ti^{3+}–C_2H_4\}$ adduct, atomic coordinates of the cluster model and periodic optimized structures.

ACKNOWLEDGMENTS

This research forms part of the research program of the Dutch Polymer Institute (DPI), project nr. 754. We acknowledge Silvia Casassa for the help with the Bader analysis and Elena Balantseva for efforts in measuring IR spectra. We are grateful to Sabine Van Doorslaer and Elio Giamello for a careful reading of the manuscript and helpful comments and suggestions.

REFERENCES

1 (a) Cossee, P. Ziegler-Natta Catalysis I. Mechanism of Polymerization of α-olefins with Ziegler-Natta Catalysts. *J. Catal.* **1964**, *3*, 80-89. (b) Arlman, E. G.; Cossee, P. Ziegler-Natta Catalysis III. Stereospecific Polymerization of Propene with the Catalyst System $TiCl_3$---$AlEt_3$. *J. Catal.* **1964**, *3*, 99-104.

2 Talarico, G.; Budzelaar, P.H.M.; Gal, A. W. Ethylene Coordination, Insertion, and Chain Transfer at a Cationic Aluminum Center: A Comparative Study with Ab Initio Correlated Level and Density Functional Methods. *J. Comput. Chem.* **2000**, *21*, 398-410.

3 Dewar, M. J. S. A Review of π Complex Theory. *Bull. Soc. Chim. Fr.* **1951**, *18*, C71-C79.

4 Chatt, J.; Duncanson, L. A. Olefin co-ordination compounds. Part III. Infra-red spectra and structure: attempted preparation of acetylene complexes. *J. Chem. Soc.* **1953**, 2939-2947.

5 Kozyra, P.; Broclawik, E.; Paweł Mitoraj, M.; Datka, J. C=C, C≡C and C=O Bond Activation by Coinage Metal Cations in ZSM-5 Zeolites: Quantitative Charge Transfer Resolution. *J. Phys. Chem. C* **2013**, *117*, 7511-7518.

6 (a) Dewar, M. J. S.; Ford, G. P. Relationship between Olefinic π Complexes and Three-membered Rings. *J. Am. Chem. Soc.* **1979**, *101*, 783-791. (b) Albright, T. A.; Hoffmann, R.; Thibeault, J. C.; Thorn, D. L. Ethylene Complexes. Bonding, Rotational Barriers, and Conformational Preferences. *Ibid.* **1979**, *101*, 3801-3812.

7 Heberhold, M. Metal ð-Complexes: Vol. II, Complexes with Mono-Olefinic Ligands; Elsevier: Amsterdam, NL, 1974

8 Huber, H.; Ozin, G. A.; Power, W. J. Modeling Catalytic Reactions with Transition Metal Atoms. 1. Synthesis and Characterization of Reactive Intermediates in the Nickel-ethylene System, (C_2H_4)nNi (where n = 1, 2, or 3) in Low Temperature Matrices. *J. Am. Chem. Soc.* **1976**, *98*, 6508-6511.

9 Merle-Mejean, T.; Cosse-Mertens, C.; Bouchareb, S.; Galan, F.; Mascetti, J.; Tranquille, M. Raman, Infrared, and UV-Visible Studles of Matrix-Isolated NiO Complexes with Ethylene, Propylene, and Butadiene. *J. Phys. Chem.* **1992**, *96*, 9148-9158.

10 Böhme, M.; Wagener, T.; Frenking, G. Copper-substituted Ethanes as a Model for Copper-acetylene Interactions on the Metal Surface. Quantum Mechanical Study of the Structure and Bonding of Copper-acetylene and Copper-ethylene Compounds $Cu_n(C_2H_2)$ (n = 1, 2, 4), $Cu(C_2H_2)^+$, $Cu_n(C_2H_4)$ (n = 1, 2) and $Cu(C_2H_4)^{+1.2}$. *J. Organomet. Chem.* **1996**, *520*, 31-43.

11 Kasai, P. H.; McLeod, D.; Watanabe, T. Acetylene and Ethylene Complexes of Copper and Silver Atoms. Matrix Isolation ESR Study. *J. Am. Chem. Soc.* **1980**, *102*, 179-190.

12 Alexander, B. D.; Dines, T. J. Ab Initio Calculations of the Structures and Vibrational Spectra of Ethene Complexes. *J. Phys. Chem. A* **2004**, *108*, 146-156.

13 Groppo, E.; Lamberti, C.; Bordiga, S.; Spoto, G.; Damin, A.; Zecchina, A. FTIR Investigation of the H_2, N_2, and C_2H_4 Molecular Complexes Formed on the Cr(II) Sites in the Phillips Catalyst: a Preliminary Step in the Understanding of a Complex System. *J. Phys. Chem. B* **2005**, *109*, 15024-15031.

14 Frenking, G.; Fröhlich, N. The Nature of the Bonding in Transition-metal Compounds. *Chem. Rev.* **2000**, *100*, 717-774.

15 Oshovsky, G. V.; Hessen, B.; Reek, J. N. H.; De Bruin, B. Electronic Selectivity Tuning in Titanium (III)-catalyzed Acetylene Cross-dimerization Reactions. *Organometallics* **2011**, *30*, 6067-6070.

16 Brozek, C. K.; Dincă, M. Ti^{3+}-, $V^{2+/3+}$-, $Cr^{2+/3+}$-, Mn^{2+}-, and Fe^{2+}-Substituted MOF-5 and Redox Reactivity in Cr-and Fe-MOF-5. *J. Am. Chem. Soc.* **2013**, *135*, 12886-12891.

17 Morra, E.; Giamello, E.; Van Doorslaer, S.; Antinucci, G.; Busico, V.; Chiesa, M. Probing the Local Environment and Coordinative Unsaturation of Ti^{3+} Species in an Activated High-Yield Ziegler Natta Catalyst. *Angew. Chem. Int. Ed.* **2015**, *54*, 4857-4860.

18 Maurelli, S.; Vishnuvarthan, M.; Chiesa, M.; Berlier, G.; Van Doorslaer, S. Elucidating the Nature and Reactivity of Ti Ions Incorporated in the Framework of AlPO-5 Molecular Sieves. New Evidence from 31P HYSCORE Spectroscopy. *J. Am. Chem. Soc.* **2011**, *133*, 7340-7343.

19 Pastore, H. O.; Coluccia, S.; Marchese, L. Porous Aluminophosphates: From Molecular Sieves to Designed Acid Catalysts. *Ann. Rev. Mater. Res.* **2005**, *35*, 351-395.

20 Raja, R.; Sankar, G.; Thomas, J. M. Bifunctional Molecular Sieve Catalysts for the Benign Ammoximation of Cyclohexanone: One-Step, Solvent-Free Production of Oxime and ε-Caprolactam with a Mixture of Air and Ammonia. *J. Am. Chem. Soc.* **2001**, *123*, 8153-8154.

21 Thomas, J. M. The Concept, Reality and Utility of Single-Site Heterogeneous Catalysts (SSHCs). *Phys. Chem. Chem. Phys.* **2014**, *16*, 7647-7661.

22 Martínez, C.; Corma, A. Inorganic Molecular Sieves: Preparation, Modification and Industrial Application in Catalytic Processes. *Coord. Chem. Rev.* **2011**, *255*, 1558-1580.

[2]3 Gómez-Hortigüela, L; Corà, F.; Catlow, C. R. A. Aerobic Oxidation of Hydrocarbons Catalyzed by Mn-Doped Nanoporous Aluminophosphates(I): Preactivation of the Mn Sites. *ACS Catal.*, **2011**, *1*, 18-28.

24 Arends, I. W. C. E.; Sheldon, R. A.; Wallau, M.; Schuchardt, U. Oxidative Transformations of Organic Compounds Mediated by Redox Molecular Sieves. *Angew. Chem., Int. Ed. Engl.* **1997**, *36*, 1144-1163.

25 Thomas, J. M.; Raja, R.; Sankar, G.; Bell, R. Molecular-Sieve Catalysts for the Selective Oxidation of Linear Alkanes by Molecular Oxygen. *Nature* **1999**, *298*, 227-230.

26 Hartmann, M.; Kevan, L.; Transition-Metal Ions in Aluminophosphate and Silicoaluminophosphate Molecular Sieves: Location, Interaction with Adsorbates and Catalytic Properties. *Chem. Rev.* **1999**, *99*, 635-664.

[2]7 Thomson, S.; Luca, V.; Howe, R. Framework Co(II) in CoAPO-5. *Phys. Chem. Chem. Phys.* **1999**, *1*, 615-619.

[2]8 Barrett, P. A.; Sankar, G.; Catlow, C. R. A.; Thomas, J. M. Investigation of the Structural Stability of Cobalt-Containing AlPO-44 Microporous Materials. *J. Phys. Chem. Solids* **1995**, *56*, 1395-1405.

[2]9 Modén, B.; Oliviero, L.; Dakka, J.; Santiesteban, J.G.; Iglesia, E. Structural and Functional Characterization of Redox Mn and Co Sites in AlPO Materials and Their Role in Alkane Oxidation Catalysis. *J. Phys. Chem. B* **2004**, *108*, 5552-5563.

30 Marchese, L.; Chen, J.S.; Thomas, J.M.; Coluccia, S.; Zecchina, A. Bronsted, Lewis, and Redox Centers on CoAPO-18 Catalysts. 1. Vibrational Modes of Adsorbed Water. *J. Phys. Chem.* **1994**, *98*, 13350-13356.

31 Saadoune, I.; Corà, F.; Catlow, C. R. A. Computational Study of the Structural and Electronic Properties of Dopant Ions in Microporous AlPOs. 1. Acid Catalytic Activity of Divalent Metal Ions. *J. Phys. Chem. B* **2003**, *107*, 3003-3011.

32 Prakash, A. M.; Kevan, L. Location and Adsorbate Interactions of Vanadium in VAPO-5 Molecular Sieve Studied by Electron Spin Resonance and Electron Spin Echo Modulation Spectroscopies. *J. Phys. Chem. B* **1999**, *103*, 2214-2222.

33 Weckhuysen, B. M.; Vannijvel, I. P.; Schoonheydt, R. A. Chemistry and Spectroscopy of Vanadium in VAPO-5 Molecular Sieves. *Zeolites* **1995**, *15*, 482-489.

34 Zahedi-Niaki, M. H.; Zaidi, S. M. J.; Kaliaguine, S. Comparative Study of Vanadium Aluminophosphate Molecular Sieves VAPO-5, -11, -17 and -31. *Appl. Catal. A-Gen.* **2000**, *196*, 9-24.

35 Fan, W. B.; Fan, B. B.; Song, M. G.; Chen, T. H.; Li, R. F.; Dou, T.; Tatsumi, T.; Weckhuysen, B. M. Synthesis, Characterization and Catalysis of (Co,V)-, (Co,Cr)- and (Cr,V)-APO-5 Molecular Sieves. *Microporous Mesoporous Mater.* **2006**, *94*, 348-357.

36 Venkatathri, N.; Shetty, V. N. Synthesis and Characterization of TAPO-31 Molecular Sieves Using Tripropylamine Template. *Catal. Commun.* **2006**, *7*, 1015-1021.

37 Maurelli, S.; Vishnuvarthan, M.; Berlier, G.; Chiesa, M. NH_3 and O_2 Interaction with Tetrahedral Ti^{3+} Ions Isomorphously Substituted in the Framework of TiAlPO-5. A Combined Pulse EPR, Pulse ENDOR, UV-Vis and FT-IR Study. *Phys. Chem. Chem. Phys.* **2012**, *14*, 987-995.

38 Gallo, E.; Piovano, A.; Marini, C.; Mathon, O.; Pascarelli, S.; Glatzel, P.; Lamberti, C.; Berlier, G. Architecture of the Ti(IV) Sites in TiAlPO-5 Determined Using Ti K-Edge X-ray Absorption and X-ray Emission Spectroscopies. *J. Phys. Chem. C* **2014**, *118*, 11745–11751.

39 Maurelli, S.; Berlier, G.; Chiesa, M.; Musso, F.; Corà, F. Structure of the Catalytic Active Sites in Vanadium-Doped Aluminophosphate Microporous Materials. New Evidence from Spin Density Studies. *J. Phys. Chem. C* **2014**, *118*, 19879-19888.

40 Morra, E.; Giamello, E.; Chiesa, M. Probing the Redox Chemistry of Titanium Silicalite-1: Formation of Tetrahedral Ti^{3+} Centers by Reaction with Triethylaluminum. *Chem. Eur. J.* **2014**, *20*, 7381-7388.

41 Höfer, P.; Grupp, A.; Nebenfür, H.; Mehring, M. Hyperfine Sublevel Correlation (HYSCORE) Spectroscopy: a 2D ESR Investigation of the Squaric Acid Radical. *Chem. Phys. Lett.* **1986**, *132*, 279-282.

42 Liesum, L.; Schweiger, A. Multiple Quantum Coherence in HYSCORE Spectra. *J. Chem. Phys.* **2001**, *114*, 9478-9488.

43 Jeschke, G.; Rakhmatullin, R.; Schweiger, A. Sensitivity Enhancement by Matched Microwave Pulses in One- and Two-dimensional Electron Spin Echo Envelope Modulation Spectroscopy. *J. Magn. Reson.* **1998**, *131*, 261-271.

44 Stoll, S.; Schweiger, A. EasySpin, a Comprehensive Software Package for Spectral Simulation and Analysis in EPR. *J. Magn. Reson.* **2006**, *178*, 42-55.

45 Corà, F.; Alfredsson, M.; Barker, C. M.; Bell, R. G.; Foster, M. D.; Saadoune, I.; Simperler, A.; Catlow, C. R. A. Modeling the Framework Stability and Catalytic Activity of Pure and Transition Metal-Doped Zeotypes. *J. Solid State Chem.* **2003**, *176*, 496-529.

46 Dovesi, R.; Orlando, R.; Civalleri, B.; Roetti, C.; Saunders, V. R.; Zicovich-Wilson, C. M. CRYSTAL: a Computational Tool for the Ab Initio Study of the Electronic Properties of Crystals. *Z. Kristallogr.* **2005**, *220*, 571-573.

47 Dovesi, R.; Saunders, V. R.; Roetti, C.; Orlando, R.; Zicovich-Wilson, C. M.; Pascale, F.; Civalleri, B.; Doll, K.; Harrison, N. M.; Bush, I. J.; D'Arco, P.; Llunell, M. *CRYSTAL09 User's Manual*; University of Torino: Torino, IT, **2009**.

48 Becke, A. D. Density-Functional Thermochemistry. 3. The Role of Exact Exchange. *J. Chem. Phys.* **1993**, *98*, 5648-5652.

49 Lee, C.; Yang, W.; Parr, R. G. Development of the Colle-Salvetti Correlation-Energy Formula into a Functional of the Electron Density. *Phys. Rev. B* **1988**, *37*, 785-789.

50 http://www.crystal.unito.it/basis-sets.php

51 Adamo, C.; Barone, V. Toward Reliable Density Functional Methods without Adjustable Parameters: The PBE0 Model. *J. Chem. Phys.* **1999**, *110*, 6158-6170.

52 Sinnecker, S.; Slep, L. D.; Bill, E.; Neese, F. Performance of Nonrelativistic and Quasi-relativistic Hybrid DFT for the Prediction of Electric and Magnetic Hyperfine Parameters in Fe-57 Mössbauer Spectra. *Inorg. Chem.* **2005**, *44*, 2245-2254.

53 Kutzelnigg, W.; Fleischer, U.; Schindler, M. *NMR Basic Principles and Progress: Vol. 23*; Springer: Berlin Heidelberg, DE, **1991**.

54 Barone, V. Structure, *Recent Advances in Density Functional Methods Part I*; World Scientific Publ. Co.: Singapore, SG, **1996**.

55 Mabbs, F. E.; Collison, D. *Electron paramagnetic resonance of d transition metal compounds*; Elsevier: Amsterdam, NL, **1992**.

56 Pöppl, A.; Kevan, L. A Practical Strategy for Determination of Proton Hyperfine Interaction Parameters in Paramagnetic Transition Metal Ion Complexes by Two-Dimensional HYSCORE Electron Spin Resonance Spectroscopy in Disordered Systems. *J. Phys. Chem.* **1996**, *100*, 3387.

57 Bader, R. F. W. *Atoms in Molecules. A Quantum Theory*; Oxford University Press: Oxford, UK, **1990**.

Table of Contents